UC Riverside

UC Riverside Previously Published Works

Title

Implementation of real-time TDDFT for periodic systems in the open-source PySCF software package

Authors

Hanasaki, Kota
Ali, Zulfikhar A
Choi, Min
et al.

SOFTWARE NOTE

Implementation of real-time TDDFT for periodic systems in the open-source PySCF software package

Kota Hanasaki[1] | Zulfikhar A. Ali[1] | Min Choi[1] | Mauro Del Ben[2] |
Bryan M. Wong[1]

[1]Department of Chemical & Environmental Engineering, Materials Science & Engineering Program, Department of Chemistry, and Department of Physics & Astronomy, University of California-Riverside, Riverside, California, USA

[2]Applied Mathematics & Computational Research Division, Lawrence Berkeley National Laboratory, Berkeley, California, USA

Correspondence

Bryan M. Wong, Department of Chemical & Environmental Engineering, Materials Science & Engineering Program, Department of Chemistry, and Department of Physics & Astronomy, University of California-Riverside, Riverside, CA, USA.
Email: bryan.wong@ucr.edu; http://www.bmwong-group.com

Abstract

We present a new implementation of real-time time-dependent density functional theory (RT-TDDFT) for calculating excited-state dynamics of periodic systems in the open-source Python-based PySCF software package. Our implementation uses Gaussian basis functions in a velocity gauge formalism and can be applied to periodic surfaces, condensed-phase, and molecular systems. As representative benchmark applications, we present optical absorption calculations of various molecular and bulk systems and a real-time simulation of field-induced dynamics of a $(ZnO)_4$ molecular cluster on a periodic graphene sheet. We present representative calculations on optical response of solids to infinitesimal external fields as well as real-time charge-transfer dynamics induced by strong pulsed laser fields. Due to the widespread use of the Python language, our RT-TDDFT implementation can be easily modified and provides a new capability in the PySCF code for real-time excited-state calculations of chemical and material systems.

KEYWORDS

electron dynamics, electron transfer, Gaussian basis, periodic systems, photophysics, real-time time-dependent density functional theory

1 | INTRODUCTION

The prediction of excited-state dynamics in condensed phase systems continues to garner immense interest due to their importance in field-induced transitions,[1,2] surface reactions,[3] photocatalysis,[4,5] nanoscale devices.[6] and strong-field dynamics.[7–9] Because of the dynamic nature of these systems, an understanding of electron dynamics at a *time-resolved* level of detail is central to improving and controlling their properties. Of the various theoretical capabilities for calculating electron dynamics, real-time time-dependent density functional theory (RT-TDDFT)[10] continues to be one the most promising computational approaches due to its balance between accuracy and cost. RT-TDDFT codes for molecular (i.e., non-periodic) systems are becoming more common since the implementation of the dipole-gauge formalism,

which is required to calculate quantum dynamics in non-periodic systems, is relatively straightforward. However, the dipole-gauge formalism cannot be used for periodic systems since it breaks the translational symmetry of the Hamiltonian.[11] As such, open-source RT-TDDFT codes for fully extended periodic systems are less common.

To bridge this gap between molecular and periodic systems, we have implemented a new RT-TDDFT capability in the open-source Python-based PySCF software package.[12] While a few RT-TDDFT implementations exist for condensed-phase systems, such as TDAP,[2] Qball,[13] Salmon,[14,15] Elk,[16] and Siesta,[17] these programs are either in-house, not open-source, or written in a low-level language. In contrast, the modular structure of the Python-based PySCF code allows easy modification and extension of built-in methodologies, even for researchers unfamiliar with specific details of each routine. These

implementations are made possible through the high-level Python language, which is known for its code readability/re-usability and has found widespread usage in the scientific community.[18] Another advantage of PySCF is its use of localized, all-electron Gaussian basis sets, which are (1) generally more accurate than pseudopotentials for RT-TDDFT calculations of intense laser fields[19] and (2) more computationally efficient for systems requiring a large vacuum space, such as extended surfaces and low-dimensional systems. Moreover, previous work has shown that efficient use of Python libraries enables PySCF to perform reasonably well for many quantum chemistry implementations,[12] although it should be re-emphasized that PySCF was designed for code readability/modularity and not massively-parallelized calculations. In the context of our work on periodic systems, the use of Gaussian basis functions and several built-in capabilities of PySCF,[12] such as the density-fitting,[20–23] enable calculations of periodic systems in a reasonable time and computational cost.

In this work, we provide a detailed description of our PySCF RT-TDDFT implementation for simulating electron dynamics of periodic systems in the presence of time-dependent external fields. To validate our custom implementation, we provide a variety of benchmark tests that include comparisons between (1) conventional linear-response and RT-TDDFT calculations, (2) different gauge choices, and (3) oscillator strength distributions. Our results are also complemented by a variety of analyses, including real-time electronic properties and time-dependent orbital occupations for a $(ZnO)_4$ molecular cluster on a periodic graphene sheet as a representative example. Finally, we conclude with a discussion and summary of our results, with additional perspectives of future applications of our RT-TDDFT implementation.

2 | METHODOLOGY

2.1 | Real-time propagation scheme

We first describe the real-time propagation scheme used in our custom PySCF implementation. We commence with the electronic ground state of a periodic system described by a given nuclear configuration with lattice vectors $\{a_i\}$ and reciprocal vectors G. Each Kohn–Sham (KS) orbital is characterized by a Bloch vector k and is a solution of the eigenvalue equation,

$$H_{\mathbf{k}}^{KS}\psi_{\mathbf{k}\alpha} = \varepsilon_{\mathbf{k}\alpha}\psi_{\mathbf{k}\alpha}, \tag{1}$$

where α is an orbital index and H^{KS} is the KS Hamiltonian given by

$$H^{KS} = \mathcal{T} + V_{ext} + V_H + V_{xc}, \tag{2}$$

where $\mathcal{T}$, V_{ext}, V_H, and V_{xc} are the kinetic energy, external potential, Hartree potential, and exchange-correlation (xc) potential operators, respectively. In this work, we focus on a Kohn–Sham treatment of the electrons (described via local and semi-local functionals), which can be readily used by PySCF developers and users without significant computational effort. We note that this formulation cannot capture all of

the intricate many-body effects in excited-state dynamics (such as electron–hole interactions), and modifications of our program to include these many-body effects would be possible future extensions of our work.

For a system is in its electronic ground state at time $t = 0$, its time evolution for future times, $t > 0$, is given by the time-dependent KS equation

$$i\hbar\frac{\partial}{\partial t}\psi_{\mathbf{k}\alpha}(\mathbf{r}, t) = H_{\mathbf{k}}^{KS}(t)\psi_{\mathbf{k}\alpha}(\mathbf{r}, t), \tag{3}$$

where $H_{\mathbf{k}}^{KS}(t)$ is the time-dependent KS Hamiltonian operator. The electron density of the system at time t is given by

$$\rho(\mathbf{r}, \mathbf{r}'; t) = \sum_{\mathbf{k}\alpha}\psi_{\mathbf{k}\alpha}(\mathbf{r}, t)w_{\mathbf{k}\alpha}\psi_{\mathbf{k}\alpha}^*(\mathbf{r}', t), \tag{4}$$

where $w_{\mathbf{k}\alpha}$ is a time-independent occupation number. In this paper, we use the adiabatic formulation[24] of TDDFT, which approximates the xc potential to be a functional of the density at time t. As representative examples of our implementation, we use local and semi-local xc functionals such as the local density approximation (LDA)[25] and the generalized gradient approximations (GGA).[26,27] We recognize that hybrid xc functionals typically give better results than LDA and GGA; however, the main purpose of our work is to validate our implementation of RT-TDDFT for periodic systems.

To numerically solve the time evolution in Equation (3), we apply the Crank–Nicolson algorithm[28] and propagate the KS orbitals as

$$\psi_{\mathbf{k}\alpha}(t + \Delta t) \approx \prod_{j=0}^{N_s-1}\left[1 + \frac{idt}{2\hbar}H_{\mathbf{k}}^{KS}\left(t_{j+\frac{1}{2}}\right)\right]^{-1}\left[1 - \frac{idt}{2\hbar}H_{\mathbf{k}}^{KS}\left(t_{j+\frac{1}{2}}\right)\right]\psi_{\mathbf{k}\alpha}(t), \tag{5}$$

where Δt is the step size of the propagation, N_s is the number of steps (typically set as $N_s = 20$ in this work), $dt \equiv \Delta t/N_s$ is the propagation time step, and $t_{j+\frac{1}{2}} \equiv t + (j+\frac{1}{2})dt$ are the time values. The Crank–Nicolson operator in Equation (5) is a strictly unitary approximation of the exact time evolution operator $e^{-i\Delta t H^{KS}/\hbar}$ for a small step size Δt. The density matrix and Hamiltonian at time $t + \Delta t$ are solved self-consistently, whereas the Hamiltonians at the intermediate time points, $H_{\mathbf{k}}^{KS}\left(t_{j+\frac{1}{2}}\right)$, are approximated by a linear interpolation of $H_{\mathbf{k}}^{KS}(t)$ and $H_{\mathbf{k}}^{KS}(t + \Delta t)$.

Within the PySCF[12] software package, the time-dependent KS orbitals are expanded in a set of Gaussian atomic orbitals (AOs) as

$$\psi_{\mathbf{k}\alpha}(\mathbf{r}, t) = \sum_{\mu}\chi_{\mathbf{k}\mu}(\mathbf{r})C_{\mathbf{k}\alpha}^{\mu}(t), \tag{6}$$

where $C_{\mathbf{k}\alpha}^{\mu}(t)$ are the time-dependent coefficients, $\chi_{\mathbf{k}\mu}(\mathbf{r}) \equiv \sqrt{\frac{1}{\mathcal{N}}}\sum_{\mathbf{T}_n}\chi_{\mu}(\mathbf{r} - \mathbf{R}_{\mu} - \mathbf{T}_n)e^{i\mathbf{k}\cdot\mathbf{T}_n}$ are the Gaussian basis functions with $\mathbf{R}_{\mu}$ being the atomic center of orbital μ, $\mathbf{T}_n$ is the lattice translation, and $\mathcal{N}$ is a formal normalization factor. The electron density, Equation (4), is expanded as

$$\rho(\mathbf{r}, \mathbf{r}'; t) = \sum_{\mathbf{k}} \sum_{\mu\nu} \chi_{\mathbf{k}\mu}(\mathbf{r}) D_{\mathbf{k}\mu\nu}(t) \chi^*_{\mathbf{k}\nu}(\mathbf{r}'), \qquad (7)$$

where $D_{\mathbf{k}\mu\nu}(t)$ is the density matrix in the AO representation, given by

$$D_{\mathbf{k}\mu\nu}(t) \equiv \sum_{\alpha} C^{\mu}_{\mathbf{k}\alpha}(t) w_{\mathbf{k}\alpha} C^{\nu*}_{\mathbf{k}\alpha}(t). \qquad (8)$$

With these definitions, the time-dependent KS equation (within the fixed nuclei approximation) in Equation (3) can be written in matrix form as

$$i\hbar \sum_{\nu} \sqrt{S}_{\mu\nu} \dot{C}^{\nu}_{\mathbf{k}\alpha}(t) = \sum_{\kappa\nu} \widetilde{H}_{\mathbf{k}\mu\kappa} \sqrt{S}_{\kappa\nu} C^{\nu}_{\mathbf{k}\alpha}(t), \qquad (9)$$

where $S_{\mu\nu}$ is the overlap matrix and $\widetilde{H}_{\mathbf{k}\mu\nu} \equiv \sum_{\sigma\kappa} \left(1/\sqrt{S}\right)_{\mu\sigma} H_{\mathbf{k}\sigma\kappa} \left(1/\sqrt{S}\right)_{\kappa\nu}$. The $C^{\nu}_{\mathbf{k}\alpha}$ coefficients can be calculated with the following expression:

$$C^{\nu}_{\mathbf{k}\alpha}(t + \Delta t) \approx \sum_{\mu\kappa} \left(\frac{1}{\sqrt{S}} \prod_{j=0}^{N_s - 1} \left[1 + \frac{i d t}{2\hbar} \widetilde{H}_{\mathbf{k}}\left(t_{j+\frac{1}{2}}\right) \right]^{-1} \left[1 - \frac{i d t}{2\hbar} \widetilde{H}_{\mathbf{k}}\left(t_{j+\frac{1}{2}}\right) \right] \right)_{\nu\mu} \left(\sqrt{S}\right)_{\mu\kappa} C^{\kappa}_{\mathbf{k}\alpha}(t). \qquad (10)$$

The required self-consistency between the KS Hamiltonian $H^{KS}(t + \Delta t)$ and the electron density $\rho(\mathbf{r}, \mathbf{r}'; t + \Delta t)$ at time $t + \Delta t$ is achieved iteratively starting from an initial guess for $H^{KS}(t + \Delta t)$. We propagate the wavefunctions using Equation (5), calculate the electron density at time $t + \Delta t$ using Equation (7), and recalculate the corresponding Hamiltonian $H^{KS}(t + \Delta t)$. This iterative procedure is repeated until a self-consistent solution is reached. We require the norm of the electron density difference across successive iterations to be smaller than a predetermined ϵ_{tol} value, which we set to 5×10^{-7}. Convergence is accelerated by Pulay's direct inversion of iterative space (DIIS) algorithm[29] in which the trial density matrix at the pth iteration step $D^{(p)}_{\mathbf{k}\mu\nu}(t)$ is set as the input vector.

2.2 | Velocity gauge formulation

The velocity gauge formulation is used to correctly incorporate the effects of external electric fields with periodic boundary conditions. In this formulation, the kinetic energy, $\mathcal{T}$, in Equation (2) becomes

$$\mathcal{T} = \frac{1}{2m_e} \left(\frac{\hbar}{i} \nabla - \frac{q_e}{c} \mathbf{A}(t) \right)^2, \qquad (11)$$

where m_e is the mass of an electron, q_e is its charge, c is the speed of light, and $\mathbf{A}(t)$ is the electromagnetic vector potential. Adopting the long-wavelength approximation and assuming the spatial uniformity of the electric field, $\mathbf{A}(t)$ is the integration of the electric field strength $\mathbf{E}(t)$: $\mathbf{A}(t) = -c \int^t dt' \mathbf{E}(t')$. The wavefunctions in the velocity gauge, ψ^{vg}, and the length gauge, ψ^{lg}, are related by a formal gauge transformation:

$$\psi^{vg}(\mathbf{r}, t) = e^{\frac{i q_e}{\hbar c} \mathbf{A}(t) \cdot \mathbf{r}} \psi^{lg}(\mathbf{r}, t). \qquad (12)$$

Non-local (NL) potentials appearing in the pseudopotential formulation are therefore transformed according to the expression

$$V^{vg}_{NL}(\mathbf{r}, \mathbf{r}') = e^{\frac{i q_e}{\hbar c} \mathbf{A}(t) \cdot \mathbf{r}} V^{lg}_{NL}(\mathbf{r}, \mathbf{r}') e^{-\frac{i q_e}{\hbar c} \mathbf{A}(t) \cdot \mathbf{r}'}. \qquad (13)$$

PySCF uses Goedecker Teter Hutter (GTH) separable dual-space pseudopotentials.[30] The matrix elements of the transformed GTH pseudopotential in a Gaussian basis set representation can be evaluated either analytically or numerically in reciprocal space. Observables containing the differential operator, such as the electronic velocity, are modified in a covariant manner as

$$\xi^{vg}(t) = \sum_{\mathbf{k}\alpha} w_{\mathbf{k}\alpha} \langle \psi^{vg}_{\mathbf{k}\alpha}(t) | \frac{1}{m_e} \left(\frac{\hbar}{i} \nabla - \frac{q_e}{c} \mathbf{A}(t) \right) + \frac{1}{i\hbar} \left[\hat{\mathbf{r}}, \ \widehat{V}^{vg}_{NL} \right] | \psi^{vg}_{\mathbf{k}\alpha}(t) \rangle, \qquad (14)$$

where the commutator term reflects the non-commutativity of the dipole and non-local pseudopotential operators.[17]

2.3 | Optical absorption spectrum

In the length gauge calculation of finite systems (i.e., molecules),[31–34] the time-dependent dipole momenta is induced by an instantaneous electric field pulse of the form $\mathbf{E}(t) = F_0 n \delta(t)$, where n is the polarization direction, F_0 the electric field amplitude, and $\delta(t)$ is the Dirac delta function. From linear response theory, the system's response to an infinitesimally small external field, $F_0 n$, is given by

$$\langle \mu^k(\mathbf{r}, \omega) \rangle = \sum_{l} \int d^3 \mathbf{r}' \chi^{kl}_0(\mathbf{r}, \mathbf{r}', \omega) n^l F_0, \qquad (15)$$

where $\mu^k(\mathbf{r}, \omega)$ is the Fourier transform of the dipole moment in the kth spatial direction at coordinate $\mathbf{r}$, where χ_0 is the response function given by

$$\chi^{kl}_0(\mathbf{r}, \mathbf{r}', \omega) = \sum_{a} \frac{\langle 0|\hat{\mu}^k(\mathbf{r})|a\rangle\langle a|\hat{\mu}^l(\mathbf{r}')|0\rangle}{\hbar\omega - E_{a0} + i\hbar\eta} - \sum_{b} \frac{\langle 0|\hat{\mu}^l(\mathbf{r}')|b\rangle\langle b|\hat{\mu}^k(\mathbf{r})|0\rangle}{\hbar\omega + E_{b0} + i\hbar\eta}, \qquad (16)$$

where $|a\rangle$ ($|0\rangle$) denotes an excited (ground) energy eigenstate with energy E_a (E_0), η is the broadening parameter, and the excitation energies are given by $E_{a0} \equiv E_a - E_0$. In our RT-TDDFT formalism, we are only interested in the spatially uniform component, and the oscillator strength can be computed as $\sum_{kl} n^k \alpha^{kl}(\omega) n^l$, where $\alpha^{kl}(\omega)$ is calculated as

$$\alpha^{kl}(\omega) \equiv -\frac{2\hbar\omega}{\pi} \mathrm{Im} \iint d^3 \mathbf{r} d^3 \mathbf{r}' \chi^{kl}_0(\mathbf{r}, \mathbf{r}'; \omega)$$
$$= 2\hbar\omega \sum_{\alpha} \langle 0|\hat{\mu}^k|\alpha\rangle\langle \alpha|\hat{\mu}^l|0\rangle \delta(\hbar\omega - E_{\alpha 0}). \qquad (17)$$

The oscillator strength satisfies the frequency sum rule. In the velocity gauge formulation, the input field transforms to a step-function vector field given by

$$\mathbf{A}(t) = -cF_0\mathbf{n}\boldsymbol{\theta}(\mathbf{t}), \qquad (18)$$

where $\theta(t)$ is the Heaviside function. In condensed-phase calculations, a convenient observable is, instead of the dipole, the electronic velocity, whose response is given by

$$\chi_{vd}^{kl}(\omega) = \sum_a \frac{\langle 0|\left[\hat{\mu}^k, \ H^{KS}\right]/i\hbar|a\rangle\langle a|\hat{\mu}^l|0\rangle}{\hbar\omega - E_{a0} + i\hbar\eta} - \sum_b \frac{\langle 0|\hat{\mu}^l|b\rangle\langle b|\left[\hat{\mu}^k, \ H^{KS}\right]/i\hbar|0\rangle}{\hbar\omega + E_{b0} + i\hbar\eta}, \qquad (19)$$

where the *vd* subscript in the previous equation indicates the dipole to velocity response. As such, Equation (17) can be succinctly written as

$$\alpha^{kl}(\omega) = -\frac{2}{\pi}\operatorname{Re}\chi_{vd}^{kl}(\omega), \qquad (20)$$

In real-time simulations, we calculate the electronic velocity (or the dipole if the target system is an isolated molecule) as a time-dependent observable, which is then Fourier-transformed to numerically calculate the response function $\chi_{vd}^{kl}(\omega)$ [$\chi^{kl}(\omega)$]. The formal expression in Equation (20) or (17) is then used to calculate the oscillator strength from the response function.

The dielectric function can be obtained from the following expression:[35]

$$\varepsilon(\omega) = 1 + \frac{4\pi i\sigma(\omega)}{\omega}, \qquad (21)$$

where the dynamical conductivity $\sigma(\omega)$ is given by

$$\sigma(\omega) = \frac{q_e}{\Omega_c}\int_{\Omega_c} d^3\mathbf{r}\int dt e^{i\omega t}\langle\Psi_t|\hat{n}\cdot\hat{\mathbf{j}}(\mathbf{r})|\Psi_t\rangle/F_0, \qquad (22)$$

where Ω_c is the cell volume, and $\hat{\mathbf{j}}(\mathbf{r})$ is the electronic current operator. The electronic current integrated over the unit cell is equivalent to the electronic velocity expectation value given in Equation (14). In our numerical implementation, the time propagation is truncated to a finite range from $0 \leq t \leq T$, where T is set to 24 fs. The time-series of dipoles/electronic velocities are multiplied by a Gaussian function of the form $e^{-w^2t^2/2}$ ($w = 0.1$ eV/$\hbar$ is used in this work) before a Fourier transformation is taken, which introduces a finite spectral width.

3 | RESULTS

This section provides numerical results of our velocity-gauge RT-TDDFT implementation in the PySCF software package. We first discuss our calculations of the optical absorption spectra and examine both non-periodic molecules (Section 3.1.1) and periodic solids

(Section 3.1.2) to validate and verify our implementation. We then discuss real-time electron dynamics between a $(ZnO)_4$ molecular cluster and a periodic graphene sheet in Section 3.2 as an example of real-time charge transfer in strong external fields.

3.1 | Optical absorption spectra

To benchmark and validate our velocity-gauge RT-TDDFT implementation, we calculated the optical absorption spectra of both molecular and condensed-phase systems. The real-time response to a vector field step-function (Equation (18)) was calculated with F_0 set to 0.001 in atomic units (a.u.). The time step, Δt, was set to 8.0 as, and the wavefunction was propagated for 3000 steps.

3.1.1 | Optical absorption spectra of molecules

As a first test of our implementation, we compare our real-time electron dynamics results for an isolated CH_4 molecule against a variety of benchmark calculations. To enable a fair and consistent comparison among the various benchmarks, all of the excited-state calculations for CH_4 were executed in the PySCF software package using the Slater exchange plus Vosko, Wilk, Nusair (S-VWN) correlation[36] and the aug-cc-pvtz[37] basis set. The molecular geometry was optimized using the Broyden–Fletcher–Goldfarb–Shanno (BFGS) variant of the Davidon–Fletcher–Powell minimization algorithm.[38]

Figure 1A compares our velocity-gauge RT-TDDFT optical absorption results against a standard linear-response (LR) TDDFT calculation. The continuous RT-TDDFT spectrum was calculated from Equation (20), and the LR-TDDFT spectrum was obtained from the tdscf module in PySCF. The low-energy optical spectrum obtained using RT-TDDFT is essentially equivalent to that obtained with LR-TDDFT, which validates our velocity-gauge implementation. As another sanity check on our implementation, we also calculated the LR-TDDFT spectrum of CH_4 with the Gaussian software package[39] at the S-VWN/aug-cc-pvtz level of theory and obtained excitation energies of 9.36, 10.40, 11.96, 12.04, 13.03, 13.67, 16.62, and 17.98 eV, which agree well with the excitation peaks shown in Figure 1A. Our next validation test is shown in Figure 1B, which compares the oscillator strength results obtained from our length-gauge and velocity-gauge RT-TDDFT calculations, using Equations (17) and (20), respectively. We obtained the length-gauge results from the system's response to a delta-function electric field strength of $F_0 = 0.001$ a.u., whereas the velocity gauge results were obtained using the Heaviside function vector field Equation (18) with the same field strength. The two results show nearly perfect agreement, indicating equivalence of the two gauge choices in the linear response regime.

Finally, Figure 1C compares the same oscillator strength distribution calculated from the dipoles and electronic velocities (see Equations (17) and (20), respectively). Except for the fictitious peak around $\omega \approx 0$ appearing in the velocity spectrum, these two results
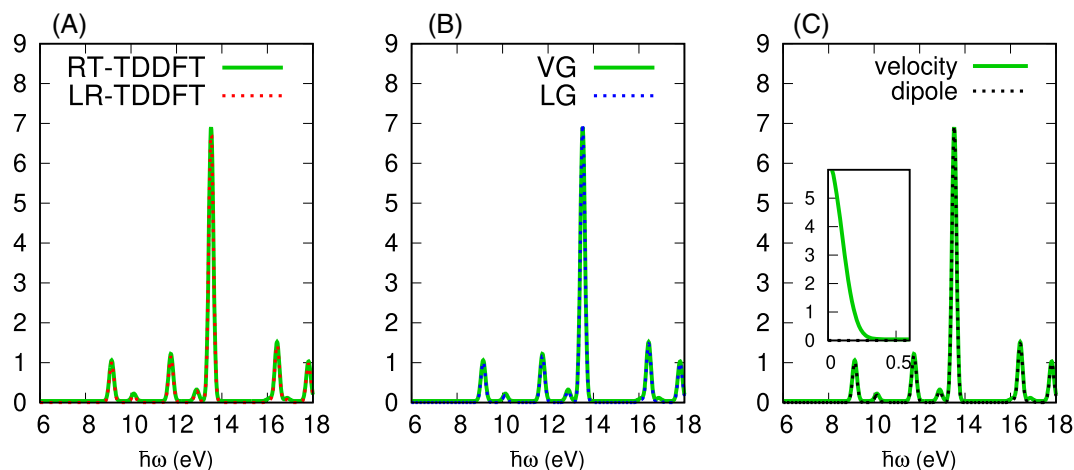
FIGURE 1 Optical absorption spectrum of the CH_4 molecule. Panel (A) shows the oscillator strength distribution of the CH_4 molecule obtained with the LDA xc potential and aug-cc-pvtz[37] basis set. The solid green line shows the RT-TDDFT result, and the dotted red line shows the LR-TDDFT result. Panel (B) shows the RT-TDDFT spectra calculated using the velocity gauge (VG, solid green line) and the length gauge (LG, dotted blue line) formulations. Panel (C) compares the velocity (solid green line) and dipole (dotted black line) spectra. The inset shows the behavior of the spectra around $\omega = 0$.
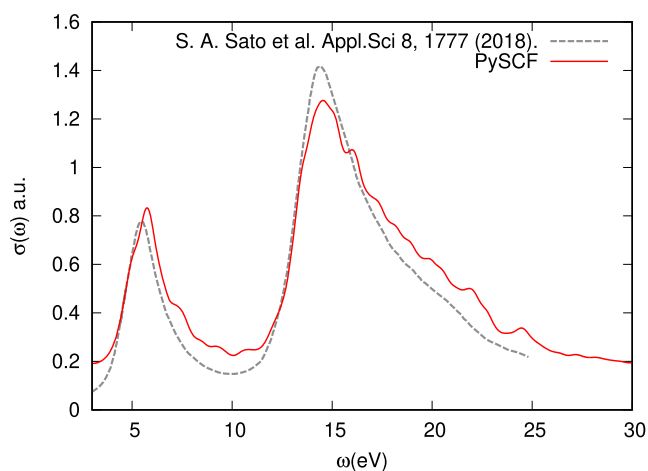

FIGURE 2 Dynamical conductivity $\sigma(\omega)$ of monolayer *h*-BN. The solid red line was obtained from our RT-TDDFT PySCF implementation, and the dashed gray line was obtained from Reference 44.

show good agreement. We attribute the appearance of the fictitious peak to the nature of the velocity spectrum calculated from Equation (20).[40] The consistency between the results obtained from the length and velocity gauges validate our RT-TDDFT implementation.

3.1.2 | Optical absorption spectra of solids

We next investigate the optical response of fully extended periodic systems. As a prototypical example, we examine a two-dimensional hexagonal boron nitride (*h*-BN) layer with a lattice constant of $a = 2.504$ Å[41] and a vacuum layer of 20 Å. We used a $15 \times 15 \times 1$ Monkhorst–Pack[42] mesh for the Brillouin zone sampling, and the

VWN[36] formulation of the LDA[25] xc functional. The GTH separable dual-space pseudopotential[30] and the double-zeta polarized basis set adapted for DFT calculations with the GTH pseudopotential (gth-dzvp)[43] was used. To enhance the computational efficiency of our calculations, the Gaussian and Plane-Wave density-fitting scheme,[23] implemented in the Fast Fourier Transformation (FFT) density-fitting routine in PySCF, was applied. In calculating the dynamical conductivity $\sigma(\omega)$, we followed the procedure in Reference 44 and introduced a damping factor of the form $e^{-\gamma t}$ with $\gamma = 0.5$ eV/$\hbar$, to reduce numerical errors due to the finite time propagation.

To further validate our implementation, we computed the dynamical conductivity of *h*-BN and compared it with the results of Reference 44. Figure 2 shows the frequency-dependent conductivity, $\sigma(\omega)$, calculated from the real-time response of the system to a weak step-function vector field in Equation (18) with $F_0 = 0.001$ a.u. and *n* in the *x* direction. Our calculation shows that our computed spectrum agrees relatively well with Reference 44, where we attribute the minor differences to the basis set and **k**-point sampling used in our calculations (Reference 44 used a real-space grid and sampled over 32×32 **k**-points). As such, the agreement between our RT-TDDFT calculations with the LDA result of Reference 44 validates our RT-TDDFT PySCF implementation for periodic systems.

3.2 | Real-time dynamics

With our PySCF RT-TDDFT implementation validated, we next discuss real-time dynamics in strong external fields. This section examines laser-induced charge transfer dynamics for a two-dimensional periodic system whose unit cell consists of a $(ZnO)_4$ molecular cluster and a 4×4 monolayer graphene sheet, which is a prototypical example of excited-state dynamics between a (non-periodic) molecule and an extended periodic system.[6]

Journal of **COMPUTATIONAL CHEMISTRY** —WILEY— **985**

Figure 3 shows our simulation cell, which consists of a 4×4 supercell of graphene and a $(ZnO)_4$ cluster, which was created with Avogadro.[45] The graphene sheet is held fixed with an inter-carbon distance of $r_{CC} = 1.42$ Å, whereas the nuclear configuration of the $(ZnO)_4$ cluster was first optimized by density functional tight binding (DFTB) calculations[46] with the 3ob parameter set[47] and subsequently shifted towards the graphene sheet by 1 Å. In this geometry, the Zn atom closest to the graphene sheet was 1.71 Å above the sheet. Our calculations utilized a single **k**-point. To reproduce the gapless excitation spectrum of graphene, we shifted the **k**-point origin by $\mathbf{K}_0 \equiv \left(\frac{4\pi}{3a}, 0, 0\right)$, where a $(= 2.4596$ Å $= 4.648$ a.u.) is the lattice constant of the graphene sheet. We applied a Fermi–Dirac distribution function corresponding to $T = 1000$ K for smearing the metallic Fermi surface. We used the Perdew, Burke, and Ernzerhof[27] GGA xc functional and the single-zeta molecularly optimized (molopt) basis set (gth-szv-molopt-sr)[43] for our RT-TDDFT calculation. Equation (10) was integrated with a time step of $\Delta t = 6$ as, and we applied an ultra-short trapezoidal pulse of width $\tau_p = 20$ fs, with an ascending/descending time of 5 fs, shown in the inset of Figure 4A. The wavelength and peak intensity of the pulse was set to $\lambda = 360$ nm and
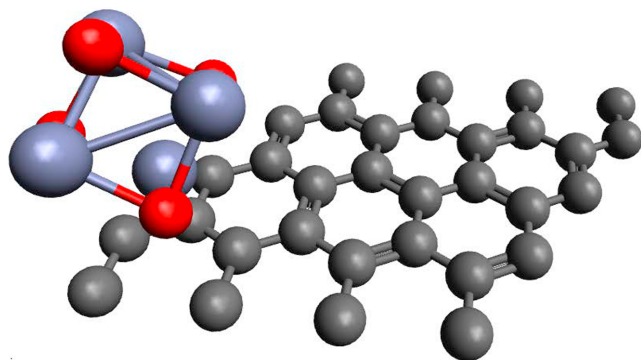
$I = 4.0 \times 10^{13}$ W/cm², respectively. We chose $\lambda = 360$ nm as our excitation energy since the local density of states of this hybrid system indicates that a UV photon with this wavelength would cause an excitation from the valence to the conduction band.

Figure 4 shows the time evolution of the electronic charges on the $(ZnO)_4$ cluster. We considered a dividing plane 1.0 Å above the graphene sheet, $z = z_0$ with $z_0 = 1.0$ Å, and defined the total electric charge Q above the dividing plane as $Q(t) \equiv \int_{z \geq z_0} dz \int \int dxdy\, \rho(\mathbf{r}, t)$, which represents the total number of electrons on the $(ZnO)_4$ cluster. Panel (A) plots the time derivative dQ/dt as a function of time. The inset in panel (A) plots the electric field of the laser pulse, which confirms that the oscillation of the electric charge on the $(ZnO)_4$ cluster is directly correlated with the oscillations of the laser field. To confirm these effects, Figure 4B plots the summation of the Mulliken charges of Zn, C, and O represented by the blue, green, and red lines, respectively. The green line represents the summation of the Mulliken charges on the carbon atoms for the entire graphene sheet. Since the total charge of the system is constant, additional charges on the carbon are provided by the $(ZnO)_4$ cluster. The oscillations of the Mulliken charges on the Zn and O atoms are partly due to charge transfer
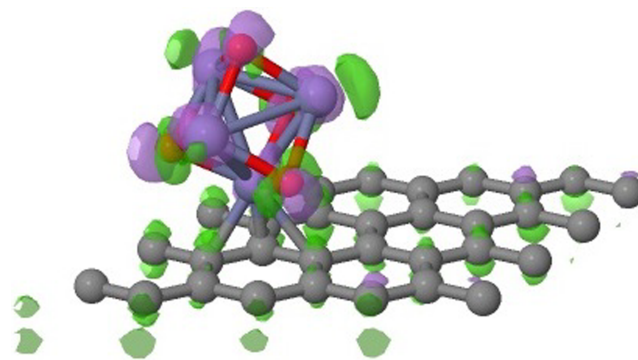

FIGURE 3 Geometry of our simulation cell consisting of a $(ZnO)_4$ molecular cluster and a 4×4 periodic graphene sheet. The purple, red, and dark gray spheres represent zinc, oxygen, and carbon atoms, respectively.

FIGURE 5 Dynamic charge transfer in a system composed of a $(ZnO)_4$ molecular cluster and a periodic graphene sheet. The charge density difference was calculated between $t = 0$ and 11.22 fs, and the green and purple isosurfaces are plotted for $\Delta\rho = \pm 0.04$ a.u.

FIGURE 4 (A) Rate of change (dQ/dt) of the total electronic charge Q above the $z = 1.0$ Å dividing plane. The inset shows the electric field of the applied laser pulse. (B) Mulliken charges as a function of time. The blue, green, and red lines track the total summation of the Mulliken charges on the zinc, carbon, and oxygen atoms, respectively.
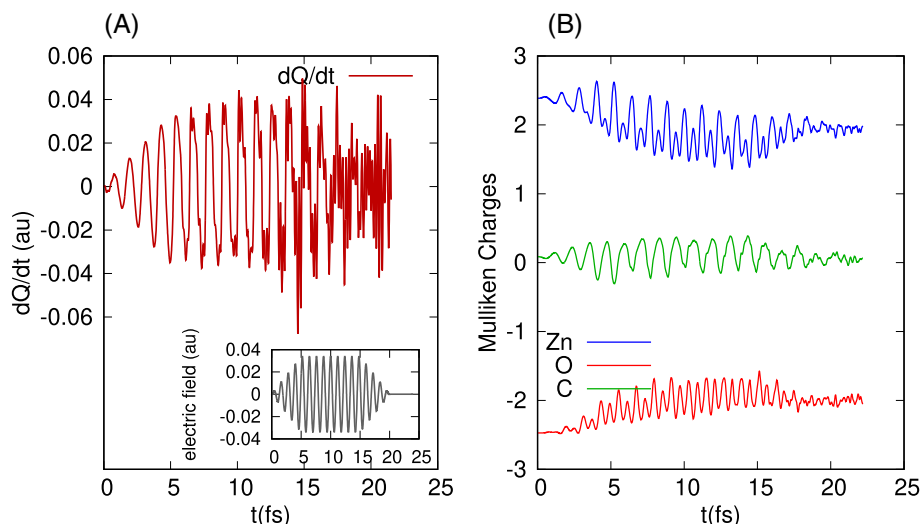
inside the $(ZnO)_4$ cluster; however, the oscillations of charge on the carbon atoms arise from charge transfer between the $(ZnO)_4$ cluster and the graphene sheet. To show the spatial distribution of the electronic density at an intermediate time $t = 11.22$ fs, Figure 5 plots the charge-density difference, $\Delta\rho(\mathbf{r}, t) \equiv \rho(\mathbf{r}, t) - \rho(\mathbf{r}, 0)$, which shows dynamic charge transfer between the $(ZnO)_4$ cluster and periodic graphene sheet.

4 | DISCUSSION AND CONCLUSION

In this work, we have implemented a new RT-TDDFT capability in the open-source Python-based PySCF software package for calculating excited-state dynamics of periodic systems. Our implementation uses Gaussian basis functions in a velocity gauge formalism and can be applied to periodic surfaces, condensed phases, and molecular systems. We have validated our custom implementation by computing optical properties of both molecular and extended periodic systems with explicit time-dependent calculations of ultrafast dynamics in these systems. Our first validation test on an isolated CH_4 molecule shows that our velocity-gauge oscillator strengths agree well with the LR-TDDFT and length-gauge TDDFT results. To validate our implementation for periodic systems, we calculated the dynamical conductivity of a periodic h-BN sheet, which agrees with previously published benchmarks. Taken together, our calculations show a close agreement between LR- and RT-TDDFT, different gauge choices, and oscillator strength distributions obtained from our time-dependent dipoles and electronic velocities. These detailed consistency tests validate our new RT-TDDFT implementation for periodic systems in the open-source PySCF software package.

With these validation tests completed, we then examined real-time, laser-induced charge-transfer dynamics for a combined $(ZnO)_4$ molecular cluster and graphene system. These results provide *real-time* mechanisms of charge transfer dynamics, which cannot be obtained from conventional linear response TDDFT approaches. Furthermore, our femtosecond laser-induced dynamics calculations for this system demonstrates that our implementation can be used to probe real-time electron dynamics in periodic systems, which is a new capability not previously available in the PySCF software package. Looking forward, we anticipate that this new capability could be used by both users and developers of RT-TDDFT for probing excited-state dynamics of periodic systems. Due to the relative simplicity and widespread use of the Python language, our RT-TDDFT implementation could be easily used/extended to other chemical and material systems, which will be incorporated in a future release of PySCF.

DATA AVAILABILITY STATEMENT

Data sharing not applicable to this article as no datasets were generated or analysed during the current study.

ORCID

Bryan M. Wong https://orcid.org/0000-0002-3477-8043

REFERENCES

[1] K. Krieger, J. K. Dewhurst, P. Elliott, S. Sharma, E. K. U. Gross, *J. Chem. Thor. Comput.* **2015**, *11*, 4870.
[2] C. Lian, S.-J. Zhang, S.-Q. Hu, M.-X. Guan, S. Meng, *Nature Commun.* **2020**, *11*, 43.
[3] Y. Zhang, S. He, W. Guo, Y. Hu, J. Huang, J. R. Mulcahy, W. D. Wei, *Chem. Rev.* **2018**, *118*, 2927.
[4] N. S. Kolobov, D. A. Svintsitskiy, E. A. Kozlova, D. S. Selishchev, D. V. Kozlov, *Chem. Eng. J.* **2017**, *314*, 600.
[5] Q. Guo, C. Zhou, Z. Ma, X. Yang, *Adv. Mat.* **2019**, *31*, 1901997.
[6] V. Q. Dang, T. Q. Trung, D.-I. Kim, L. T. Duy, B.-U. Hwang, D.-W. Lee, B. Y. Kim, L. D. Toan, N.-E. Lee, *Small* **2015**, *11*, 3054.
[7] G. Vampa, C. R. McDonald, G. Orlando, P. B. Corkum, T. Brabec, *Phys. Rev. B* **2015**, *91*, 64302.
[8] I. Floss, C. Lemell, G. Wachter, V. Smejkal, S. A. Sato, X.-M. Tong, K. Yabana, J. Burgdorfer, *Phys. Rev. A* **2018**, *97*, 11401.
[9] N. Tancogne-Dejean, O. D. Mücke, F. X. Kartner, A. Rubio, *Phys. Rev. Lett.* **2017**, *118*, 87403.
[10] E. Runge, E. K. U. Gross, *Phys. Rev. Lett.* **1984**, *52*, 997.
[11] R. D. King-Smith, D. Vanderbilt, *Phys. Rev. B* **1993**, *47*, 1651.
[12] Q. Sun, T. C. Berkelbach, N. S. Blunt, G. H. Booth, S. Guo, Z. Li, J. Liu, J. D. McClain, E. R. Sayfutyarova, S. Sharma, S. Wouters, G. K.-L. Chan, *WIREs Comput. Mol. Sci.* **2018**, *8*, 1340.
[13] J. Sun, C.-W. Lee, A. Kononov, A. Schleife, C. A. Ullrich, *Phys. Rev. Lett.* **2021**, *127*, 077401.
[14] K. Yabana, T. Nakatsukasa, J.-I. Iwata, G. F. Bertsch, *Phys. Stat. Sol. (b)* **2006**, *243*, 1121.
[15] M. Noda, S. A. Sato, Y. Hirokawa, M. Uemoto, T. Takeuchi, S. Yamada, A. Yamada, Y. Shinohara, M. Yamaguchi, K. Iida, I. Floss, T. Otobe, K.-M. Lee, K. Ishimura, T. Boku, G. F. Bertsch, K. Nobusada, K. Yabana, *Comput. Phys. Commun.* **2019**, *235*, 356.
[16] J. Dewhurst K. Krieger, K. Sharma, S. Gross, Computational Physics, **2014**. http://arxiv.org/abs/1412.0996.
[17] C. D. Pemmaraju, F. D. Vila, J. J. Kas, S. A. Sato, J. Rehr, K. Yabana, D. Prendergast, *Comput. Phys. Commun.* **2018**, *226*, 30.
[18] Z. Merali, *Nature* **2010**, *467*, 775.
[19] X.-M. Tong, G. Wachter, S. A. Sato, C. Lemell, K. Yabana, J. Burgdörfer, *Phys. Rev. A* **2015**, *92*, 043422.
[20] J. L. Whitten, *J. Chem. Phys.* **1973**, *58*, 4496.
[21] F. Weigend, *Phys. Chem. Chem. Phys.* **2006**, *8*, 1057.
[22] Q. Sun, T. C. Berkelbach, J. D. McClain, G. K.-L. Chan, *J. Chem. Phys.* **2017**, *147*, 164119.
[23] G. Lippert, J. Hutter, M. Parrinello, *Mol. Phys.* **1997**, *92*, 477.
[24] M. Thiele, E. K. U. Gross, S. Kümmel, *Phys. Rev. Lett.* **2008**, *100*, 153004.
[25] W. Kohn, L. J. Sham, *Phys. Rev.* **1965**, *140*, A1133.
[26] J. P. Perdew, Y. Wang, *Phys. Rev. B* **1992**, *45*, 13244.
[27] J. P. Perdew, K. Burke, M. Ernzerhof, *Phys. Rev. Lett.* **1996**, *77*, 3865.
[28] J. Crank, P. Nicolson, *Proc. Camb. Phil. Soc.* **1947**, *43*, 50.
[29] (a) P. Pulay, *Chem. Phys. Lett.* **1980**, *73*, 393; (b) ibid, *J. Comput. Chem.* **1982**, *3*, 556.
[30] S. Goedecker, M. Teter, J. Hutter, *Phys. Rev. B* **1996**, *54*, 1703.
[31] M. B. Oviedo, B. M. Wong, *J. Chem. Theory Comput.* **2016**, *12*, 1862.
[32] N. V. Ilawe, M. B. Oviedo, B. M. Wong, *J. Chem. Theory Comput.* **2017**, *13*, 3442.

[33] N. V. Ilawe, M. B. Oviedo, B. M. Wong, _J. Mater. Chem. C_ **2016**, _6_, 5857.

[34] J. M. Rodríguez-Borbón, A. Kalantar, S. S. R. K. K. Yamijala, M. B. Oviedo, W. Najjar, B. M. Wong, _J. Chem. Theory Comput._ **2020**, _16_, 2085.

[35] K. Yabana, T. Sugiyama, Y. Shinohara, T. Otobe, G. F. Bertsch, _Phys. Rev. B_ **2012**, _85_, 45134.

[36] S. Vosko, L. Wilk, M. Nusair, _Can. J. Phys._ **1980**, _58_, 1200.

[37] T. H. Dunning, _J. Chem. Phys._ **1989**, _90_, 1007.

[38] V. H. Press, S. A. Teukolsky, W. T. Vetterling, B. P. Flannery, Numerical Recipes in C Cambridge, **1999**, 428.

[39] M. J. Frisch, G. W. Trucks, H. B. Schlegel, G. E. Scuseria, M. A. Robb, J. R. Cheeseman, G. Scalmani, V. Barone, B. Mennucci, G. A. Petersson, H. Nakatsuji, M. Caricato, X. Li, H. P. Hratchian, A. F. Izmaylov, J. Bloino, G. Zheng, J. L. Sonnenberg, M. Hada, M. Ehara, K. Toyota, R. Fukuda, J. Hasegawa, M. Ishida, T. Nakajima, Y. Honda, O. Kitao, H. Nakai, T. Vreven, J. A. Montgomery, J. E. Peralta, F. Ogliaro, M. Bearpark, J. J. Heyd, E. Brothers, K. N. Kudin, V. N. Staroverov, R. Kobayashi, J. Normand, K. Raghavachari, A. Rendell, J. C. Burant, S. S. Iyengar, J. Tomasi, M. Cossi, N. Rega, J. M. Millam, M. Klene, J. E. Knox, J. B. Cross, V. Bakken, C. Adamo, J. Jaramillo, R. Gomperts, R. E. Stratmann, O. Yazyev, A. J. Austin, R. Cammi, C. Pomelli, J. W. Ochterski, R. L. Martin, K. Morokuma, V. G. Zakrzewski, G. A. Voth, P. Salvador, J. J. Dannenberg, S. Dapprich, A. D. Daniels, Ö Farkas, J. B. Foresman, J. V. Ortiz, J. Cioslowski, D. J. Fox, Gaussian 09 Revision C.01, **2011**.

[40] From Eqs. (17) and (20), it is clear that the dipole spectrum vanishes at $\omega = 0$ while that of the velocity does not necessarily. The latter can take a finite value at $\omega = 0$ because of numerical errors arising from the finite-range Fourier transformation.

[41] L. Liu, Y. P. Feng, Z. X. Shen, _Phys. Rev. B_ **2003**, _68_, 104102.

[42] H. J. Monkhorst, J. D. Pack, _Phys. Rev. B_ **1976**, _13_, 5188.

[43] J. VandeVondele, J. Hutter, _J. Chem. Phys._ **2007**, _127_, 114105.

[44] S. A. Sato, H. Hübener, U. De Giovannini, A. Rubio, _App. Sci._ **2018**, _8_, 1777.

[45] M. D. Hanwell, D. E. Curtis, D. C. Lonie, T. Vandermeersch, E. Zurek, G. R. Hutchison, J. Cheminfo. 4, 17; Avogadro: an open-source molecular builder and visualization tool. Version 1.2.0. **2012**. http://avogadro.cc/.

[46] B. Aradi, B. Hourahine, T. Frauenheim, _J. Phys. Chem. A_ **2007**, _111_, 5678.

[47] M. Gaus, A. Goez, M. Elstner, _J. Chem. Theor. Comput._ **2013**, _9_, 338. X. Lu, M. Gaus, M. Elstner, Q. Cui, _J. Phys. Chem. B_ **2015**, _119_, 1062.

How to cite this article: K. Hanasaki, Z. A. Ali, M. Choi, M. Del Ben, B. M. Wong, _J. Comput. Chem._ **2023**, _44_(9), 980. https://doi.org/10.1002/jcc.27058